Synthesis and Structure of Low-Dimensional Gallium Fluorodiphosphates Seen during the Crystallization of the Three-Dimensional Microporous Gallium Fluorophosphate ULM-3

Franck Millange,*[,†] Richard I. Walton,[‡] Nathalie Guillou,[†] Thierry Loiseau,[†] Dermot O'Hare,[§] and Gérard Férey*[,†]

Institut Lavoisier, UMR CNRS 8637, Université de Versailles Saint-Quentin-en-Yvelines, 45 Avenue des Etats-Unis, 78035 Versailles Cedex, France, School of Chemistry, University of Exeter, Stocker Road, Exeter, Devon EX4 4QD, United Kingdom, and Inorganic Chemistry Laboratory, University of Oxford, South Parks Road, Oxford OX1 3QR, United Kingdom

Received June 14, 2002. Revised Manuscript Received July 25, 2002

Two one-dimensional gallium fluorodiphosphates $Ga(P_2O_7)F{\cdot}H_3N(CH_2)_3NH_3{\cdot}3H_2O$, **1**, and $Ga(P_2O_7)F{\cdot}H_3N(CH_2)_3NH_3{\cdot}H_2O$, **2**, have been synthesized under mild conditions (<100 °C) from aqueous mixtures of $Ga(NO_3)_3{\cdot}6H_2O$, P_2O_5, 1,3-diaminopropane, and HF. Their structures consist of anionic chains of formula $Ga(P_2O_7)F^{2-}$ containing corner-sharing $\{GaO_4F_2\}$ octahedra linked together via fluorine and P_2O_7 units, which are charge-balanced by propyldiammonium dications. During the hydrothermal synthesis of the open-framework three-dimensional ULM-3, compound **2** has been identified as the crystalline intermediate phase when phosphorus pentoxide is used as a starting material. This process has been followed in situ with time-resolved energy-dispersive X-ray diffraction (EDXRD), which reveals that dissolution of the one-dimensional phase **2** occurs before the rapid crystallization of ULM-3. If compound **2** is quenched from hydrothermal conditions, rapid and reversible conversion to compound **1** takes place. The two chain phases are thus solid precursors of the microporous ULM-3, and tracking the transformation process using in situ EXDRD shows that dissolution of **1** takes place before crystallization of **2** and then further transformation into the 3D phase, with the **1** and **2** acting as reservoirs of reactive species for ULM-3 crystallization.

Introduction

The discovery of aluminum phosphates with zeolite-like structures in 1982[1] brought about a huge amount of research into the synthesis of new microporous solids. This work is driven by the diverse commercial applications of the solids in areas such as shape-selective catalysis, ion exchange, and gas separation (molecular sieving). The microporous phosphates now include solids that contain elements from all groups of the periodic table (ranging from main group elements such as Mg, Ga, In, and Zn to transition metals such as Fe, Mn, and Co).[2] These materials remain the focus of attention, first, because they exhibit structures not seen in silicate zeolite chemistry (for example, containing nontetrahedral constituent polyhedra with coordination numbers higher than four) and, second, because the inclusion of chemically active metal centers in phosphate frameworks can infer unusual catalytic activity (for example, the synthesis of highly active and selective aerial oxidation catalysts based on transition-metal phosphates has recently been described).[3] As well as the substitution of the metal centers in microporous phosphates, another successful tactic in the preparation of new materials has been the incorporation of fluoride into the open-framework materials. This method was first introduced by Guth et al.,[4] and as well as acting as a mineralizing agent (improving crystallinity of the solid products), fluoride is often included in the constituent coordination polyhedra, bringing about great structural variety. The ULM-*n* and MIL-*n* families of fluorophosphates, discovered by some of us, are the largest group of fluorine-including phosphates[5,6] and include microporous phases of the metals Al, Ga, Fe, V, and Ni, the majority of which have structures not seen in the zeolites and several of which have the largest pore sizes seen for open-framework phosphates (for example, VSB-1 and VSB-5 exhibit 24-membered ring tunnels).[7,8]

* To whom correspondence should be addressed. E-mails: millange@chimie.uvsq.fr; ferey@chimie.uvsq.fr.
† Université de Versailles Saint-Quentin-en-Yvelines.
‡ University of Exeter.
§ University of Oxford.

(1) Wilson, S. T.; Lok, B. M.; Messina, C. A.; Cannan, T. R.; Flanigen, E. M. *J. Am. Chem. Soc.* **1982**, *104*, 1146.
(2) Cheetham, A. K.; Férey, G.; Loiseau, T. *Angew. Chem. Int. Ed.* **1999**, *38*, 3269.
(3) Thomas, J. M.; Raja, R.; Sankar, G.; Bell, R. G. *Acc. Chem. Res.* **2001**, *34*, 191.
(4) Guth, J. L.; Kessler, H.; Wey, R. *Stud. Surf. Sci. Catal.* **1986**, *28*, 121.
(5) Férey, G. *J. Fluor. Chem.* **1995**, *72*, 187.
(6) Férey, G. *C. R. Acad. Sci. Paris Ser. IIc* **1998**, *1*, 1.
(7) Guillou, N.; Gao, Q.; Noguès, M.; Morris, R. E.; Hervieu, M.; Férey, G.; Cheetham, A. K. *C. R. Acad. Sci. Paris Ser. IIc* **1999**, *2*, 387.

10.1021/cm021232v CCC: $22.00
Published on Web 09/14/2002

Table 1. Reactions Performed in the Current Work[a]

composition of starting mixture	reaction conditions	product
Ga_2O_3:P_2O_5:1.9DAP:2.0HF:70H_2O	25 °C, 1 week	$Ga(P_2O_7)F{\cdot}H_3N(CH_2)_3NH_3{\cdot}3H_2O$ **(1)** + GaOOH
0.5$Ga(NO_3)_3{\cdot}xH_2O$:3P_2O_5:5.4DAP:6.0HF:208H_2O	90 °C, 4 days	$Ga(P_2O_7)F{\cdot}H_3N(CH_2)_3NH_3{\cdot}3H_2O$ **(1)**
0.5$Ga(NO_3)_3{\cdot}xH_2O$:3P_2O_5:5.4DAP:6.0HF:H_2O/EG	90 °C, 4 days	$Ga(P_2O_7)F{\cdot}H_3N(CH_2)_3NH_3{\cdot}H_2O$ **(2)**

[a] The Ga_2O_3 starting material (Aldrich 99.9%) was shown by X-ray diffraction to contain crystalline GaOOH, which will not react. DAP is 1,3-diaminopropane and EG is ethylene glycol. Product identification was based on powder X-ray diffraction.

A pressing aim in the area of microporous materials is the need to understand the formation mechanism of the solids.[9,10] This knowledge would enable new materials to be prepared rationally by application of precisely controlled reaction conditions; for example, it would be possible to synthesize a framework with pore sizes and polarity required by a particular catalytic application. Microporous solids are commonly prepared using the hydrothermal route, involving crystallization from a heterogeneous mixture of solid and liquid reagents with a solvent in a sealed reaction container heated above the boiling point of the mixture. The requirement for thick-walled reaction vessels in hydrothermal synthesis means that the acquisition of kinetic and mechanistic information concerning the crystallization of microporous solids is extremely difficult to achieve. We have recently been at the forefront of the development of new in situ methodologies to allow the monitoring of physical and chemical changes within hydrothermal autoclaves: this has included diffraction methods[11−13] and in situ NMR techniques.[14] We have used these techniques to track the crystallization of aluminum and gallium phosphates belonging to the ULM-*n* family: NMR studies have revealed the presence of prenucleation building units in solution,[14] whereas in situ diffraction studies have permitted accurate crystallization curves to be deduced and the observation of transient crystalline phases during crystallization.[15−17] These data are the first that will allow the crystallization mechanism to be experimentally deduced for this family of materials and our work is of relevance to the work focused on the formation mechanism of related solids, such as the aluminum phosphates studied by Ozin and co-workers[18] and the zinc phosphates studied by Rao and coworkers.[19]

Until now we have been unable to characterize fully the crystalline intermediate phases we observed during our in situ studies: the energy-dispersive X-ray diffraction (EDXRD) technique that we used produces data that are inherently of low resolution and therefore not suitable for structure solution, and on quenching the reaction mixtures when an intermediate is present, it is observed that the transient phases undergo transformation to other crystalline solids. The structures of the intermediate materials would clearly be of great importance in understanding the pathways leading to the formation of microporous materials. In this paper we describe the first successful isolation and structure solution of a phase previously only seen in situ using EDXRD during the formation of microporous ULM-3. A second phase, which readily transforms into the transient intermediate, is also described: both have 1D structures and may be thought of as precursors to the microporous 3D solid. We have recently published a preliminary description of the structures of these phases;[20] herein, we describe their synthesis, their ab initio structure solution from powder X-ray diffraction data, and the results of an in situ EDXRD study of their hydrothermal behavior.

Experimental Section

Synthesis. Syntheses were carried out at room temperature or under mild hydrothermal conditions using gallium oxide (Ga_2O_3, 99.99%, Aldrich), gallium nitrate hydrate ($Ga(NO_3)_3{\cdot}xH_2O$, 99.9%, Aldrich), diphosphorus pentoxide (P_2O_5, 97%, Prolabo), hydrofluoric acid (HF, 48% in water, Prolabo), 1,3-diaminopropane, denoted DAP, ($H_2N(CH_2)_3NH_2$, 99%, Aldrich), ethylene glycol, denoted EG, ($C_2H_6O_2$, 99.5%, Fluka), and deionized water. Table 1 shows the initial compositions of reaction mixtures used and the conditions applied.

$Ga(P_2O_7)F{\cdot}H_3N(CH_2)_3NH_3{\cdot}3H_2O$, **1**, was initially prepared by simply standing at room temperature a reaction mixture usually heated in a hydrothermal bomb to prepare ULM-3 $Ga_3(PO_4)_3F_2{\cdot}H_3N(CH_2)_3NH_3{\cdot}H_2O$ (see reaction 1, Table 1). Ga_2O_3 was used as the gallium source and the mixture was placed in a Teflon tube covered with film after thorough stirring. A laboratory powder X-ray diffraction pattern of the solid product after recovering and washing with water showed that a novel crystalline phase had been produced, although contaminated with a small amount of unreacted GaOOH present in the Ga_2O_3 starting material. Interestingly, if the reaction mixture was not thoroughly stirred, large single crystals (up to 2 mm in dimension) were produced; determination of the cell parameters of one of these revealed the material to be $[NH_3(CH_2)_3NH_3]P_4O_{12}{\cdot}2H_2O$,[21] and this identification was confirmed by powder X-ray diffraction analysis of a ground sample of the crystallites. A sample of the phosphorus-rich gallium fluorophosphate was subsequently prepared in pure form, by adjusting the composition of the reaction mixture. To avoid the presence of the unreacted GaOOH, Ga_2O_3 was replaced by $Ga(NO_3)_3{\cdot}6H_2O$ (see reaction 2, Table 1) and the Ga:P ratio in the initial gel was changed to be 1:12, the amount of HF tripled, and the pH adjusted by

(8) Guillou, N.; Gao, Q.; Forster, P. M.; Chang, J. S.; Noguès, M.; Park, S. E.; Férey, G.; Cheetham, A. K. *Angew. Chem. Int. Ed.* **2001**, *40*, 2831.
(9) Cheetham, A. K.; Mellot, C. F. *Chem. Mater.* **1997**, *9*, 2269.
(10) Francis, R. J.; O'Hare, D. *J. Chem. Soc., Dalton Trans.* **1998**, 3133.
(11) Walton, R. I.; O'Hare, D. *Chem. Commun.* **2000**, 2283.
(12) Walton, R. I.; Francis, R. J.; Halasyamani, P. S.; O'Hare, D.; Smith, R. I.; Done, R.; Humpreys, R. J. *Rev. Sci. Instrum.* **1999**, *70*, 3391.
(13) Evans, J. S. O.; Francis, R. J.; O'Hare, D.; Price, S. J.; Clarke, S. M.; Flaherty, J.; Gordon, J.; Nield, A.; Tang, C. C. *Rev. Sci. Instrum.* **1995**, *66*, 2442.
(14) Haouas, M.; Gerardin, C.; Taulelle, F.; Estournes, C.; Loiseau, T.; Férey, G. *J. Chim. Phys.* **1997**, *95*, 302.
(15) Walton, R. I.; Loiseau, T.; O'Hare, D.; Férey, G. *Chem. Mater.* **1999**, *3201*, 1.
(16) Francis, R. J.; Price, S. J.; O'Brien, S.; Fogg, A. M.; O'Hare, D.; Loiseau, T.; Férey, G. *Chem. Commun.* **1997**, 521.
(17) Francis, R. J.; O'Brien, S.; Fogg, A. M.; Halasyamani, P. S.; O'Hare, D.; Loiseau, T.; Férey, G. *J. Am. Chem. Soc.* **1999**, *121*, 1002.
(18) Oliver, S.; Kuperman, A.; Ozin, G. A. *Angew. Chem., Int. Ed.* **1998**, *37*, 46.
(19) Rao, C. N. R.; Natarajan, S.; Choudhury, A.; Neeraj, S.; Ayi, A. A. *Acc. Chem. Res.* **2001**, *24*, 80.
(20) Millange, F.; Walton, R. I.; Guillou, N.; Loiseau, T.; O'Hare, D.; Férey, G. *Chem. Commun.* **2002**, 826.
(21) Bdiri, M.; Jouini, A. *Acta Crystallogr. C* **1990**, *46*, 1454.

the addition of the appropriate amount of 1,3-diaminopropane to be the same as that initially used. The mixture was held at 90 °C for 4 days. The strongest Bragg reflection of GaOOH was not observed in the powder pattern of this sample. It has not been possible to prepare crystals of suitable size for single-crystal diffraction studies; for example, if the reaction mixture stood for longer periods (up to several months), no change in the sample nature was observed and seeding the mixture with pre-made sample afforded no larger crystals.

$Ga(P_2O_7)F{\cdot}H_3N(CH_2)_3NH_3{\cdot}H_2O$, **2**, was prepared under mild hydrothermal conditions using a mixed water/EG solvent (see reaction 3, Table 1): 0.187 g of $Ga(NO_3)_3{\cdot}6H_2O$, 0.439 g of P_2O_5, 0.250 g of HF (48%), 0.401 g of 1,3-diaminopropane, 3.744 g of H_2O, and 3.744 g of EG were sealed in a Teflon-lined autoclave and heated at 90 °C for 4 days. The white solid product was recovered by filtration, washed with deionized water, and dried at room temperature. Traces of $Ga(P_2O_7)F{\cdot}H_3N(CH_2)_3NH_3{\cdot}3H_2O$, **1**, which also crystallizes from the same reactants, were observed with $Ga(P_2O_7)F{\cdot}H_3N(CH_2)_3NH_3{\cdot}H_2O$, **2**, by powder X-ray diffraction.

Electron Microscopy. A JEOL 2000FX transmission electron microscope was used, equipped with a Link "Pentafet" EDX detector (Be window), and attached to an eXL hardware interface. A highly crystalline sample of $GaPO_4$, prepared by hydrothermal reaction between Ga_2O_3 and H_3PO_4, was studied to calculate a calibration constant to relate the relative atomic concentration of gallium and phosphorus to the observed ratios of intensities of gallium-L and phosphorus-K X-ray emissions (the ratio method). Typically, 15 crystallites of each sample were analyzed. X-ray microanalysis showed the platelike crystallites of **1** and **2** to contain Ga and P in the ratio 1:2, and emissions characteristic of O, F, C, and N were observed.

Elemental Analysis. Compound **1** elemental analysis gave the following results: Ga, 17.61%; P, 15.35%; F, 4.61%; C, 9.38%; N, 7.28%; H, 4.60%. These values compare well with those calculated from the proposed formula $Ga(P_2O_7)F{\cdot}H_3N(CH_2)_3NH_3{\cdot}3H_2O$, **1**: Ga, 17.81%; P, 15.77%; F, 4.83%; C, 9.16%; N, 7.12%; H, 4.58%. Similar results found for compound **2** indicate that the contents of Ga, P, F, C, N, and H are in good agreement with the values based on the structure formula.

Thermogravimetry. Thermogravimetric analysis was carried out on a TGA Instrument type 2050 thermoanalyzer, under oxygen gas flow with a heating rate of 5 °C min^{-1} from 25 to 600 °C.

Powder X-ray Diffraction. A number of powder X-ray diffraction methods were used to characterize the materials:

Energy-dispersive X-ray diffraction experiments were performed on Station 16.4 of the Daresbury SRS using apparatus previously described.[13] Station 16.4 is illuminated with radiation from a 6T superconducting wiggler insertion device and receives X-rays over an energy range of 5−120 keV with a maximum X-ray flux of 3×10^{10} photons/s at around 13 keV. The high-intensity, white X-ray beam allows the penetration of thick-walled reaction vessels, and the fixed detector provides rapid data acquisition (<1 min). Thus, in situ, time-resolved diffraction studies of chemical processes are possible under genuine laboratory conditions: a hydrothermal reaction cell which has a similar volume to those available commercially for laboratory use (~25 mL), but a thinner stainless steel outer case (0.4 mm) to minimize absorption of X-rays, was used for the current work. In a typical reaction, 1 g of metal source was dispersed in 10 cm^3 of deionized water by stirring with use of a magnetic flea. The phosphorus source, hydrofluoric acid, and finally the amine were added; the mixture was stirred for a few moments, then sealed in the cell, and transferred to the preheated apparatus. The reaction mixture was continually stirred during data collection to ensure solid material remained in the beam at all times and did not settle out. X-ray diffraction patterns were recorded every 30 s by a three-element, solid-state detector.[22] For the energy-dispersive diffraction experiment, E (keV) = 6.19926/(d sin θ) for a Bragg reflection arising from a plane of d (in Å). A preprepared sample of the open-framework three-dimensional ULM-3 was stirred in 10 cm^3 of water with the hydrothermal cell and the position of at least four strong and well-resolved Bragg reflections were used to determine accurately the angle of each detector (2θ). In the experiments described, the detector angles were 1.87°, 4.64°, and 7.40°.

Temperature-dependent X-ray powder diffraction measurements were performed using a Siemens D5000 diffractometer ($\theta-\theta$ mode, Co Kα radiation λ = 1.7903 Å) equipped with an Anton Paar HTK16 high-temperature device and a M Braun linear position-sensitive detector (PSD) under static air. Patterns were scanned with a resolution of 0.0147° and a divergence slit of 0.1° over the angular range 2θ = 7−40° to observe the most intense low-angle Bragg reflections. Temperature steps of 10 °C from 30 to 100 °C and of 20 °C thereafter up to 600 °C were typically used.

Ambient X-ray powder diffraction data of the new compounds were collected on a Siemens D5000 diffractometer using Cu Kα radiation (λ = 1.5418 Å). To minimize preferred orientation effects, the powder was ground in ethanol with a "McCrone" grinder, dried at room temperature, and then side-loaded in the sample holder. The powder diffraction patterns were scanned over the angular range of 7−100° (2θ) and 7−90° (2θ) for **1** and **2,** respectively, with a step size of 0.02° (2θ). The counting times were 29.5 s $step^{-1}$ to 41.98° (2θ) and 59 s $step^{-1}$ in the 42−100° (2θ) range for **1**; 32.5 s $step^{-1}$ to 33.98° (2θ) and 65 s $step^{-1}$ in the 34−90° (2θ) range for **2**. This procedure was used to improve the counting statistics of the high-angle region. Then, full patterns were scaled to the lower counting time.

Results

Structure Solution. Since no suitable single crystals of either phase were obtained, an ab initio structure determination from powder diffraction was carried out for each. A determination of the peak positions for Cu $K\alpha_1$ radiation contribution was carried out by means of the WinPLOTR program.[23] Pattern indexing was then performed by means of the computer program DICVOL91[24] from the first 20 lines, with an absolute error in peak positions of 0.03° (2θ). Satisfactory figures of merit[25,26] (see Table 2) were thus obtained for both compounds. **1** crystallizes with a primitive monoclinic cell [a = 9.569(3) Å, b = 7.166(3) Å, c = 9.996(4) Å, β = 108.80(4)°] while **2** crystallizes with a centered orthorhombic cell [a = 10.311(1) Å, b = 15.949(1) Å, c = 7.224(1) Å]. The refined lattice constants are given in Table 2. It should be noted that a primitive monoclinic cell could also be found for compound **2** with the cell parameters [a = 9.496(1) Å, b = 7.224(1) Å, c = 10.311(1) Å, β = 122.89(4)°], close to those determined for compound **1**. However, a check for possible higher metrical symmetries of the lattice using the Lepage code led to the centered orthorhombic cell. The relationship between the two cells is the following: $a_{ortho} = c_{mono}$, $b_{ortho} = (4a_{mono}^2 - c_{mono}^2)^{1/2}$, and $c_{ortho} = b_{mono}$. No higher symmetry could be detected for compound **1**. A structureless whole pattern profile refinement by the Le Bail method[27] program FullProf[28] confirmed the adequacy

(22) Colston, S. L.; Jacques, S. D. M.; Barnes, P.; Jupe, A. C.; Hall, C. *J. Synchrotron Radiat.* **1998**, *5*, 112.

(23) Roisnel, T.; Rodriguez-Carvajal, J. In *Abstracts of the 7th European Powder Diffraction Conference*, Barcelona, Spain, 2000; p 71.

(24) Boultif, A.; Louër, D. *J. Appl. Crystallogr.* **1991**, *24*, 987.

(25) de Wolff, P. M. *J. Appl. Crystallogr.* **1972**, *5*, 243.

(26) Smith, G. S.; Snyder, R. L. *J. Appl. Crystallogr.* **1979**, *12*, 60.

(27) Le Bail, A.; Duroy, H.; Fourquet, J. *Mater. Res. Bull.* **1988**, *23*, 447.

Table 2. Crystal Data and Structure Refinement Parameters for $Ga(P_2O_7)F{\cdot}H_3N(CH_2)_3NH_3{\cdot}3H_2O$ (1) and $Ga(P_2O_7)F{\cdot}H_3N(CH_2)_3NH_3{\cdot}H_2O$ (2)

formula	$Ga(P_2O_7)F{\cdot}H_3N(CH_2)_3NH_3{\cdot}3H_2O$ **(1)**	$Ga(P_2O_7)F{\cdot}H_3N(CH_2)_3NH_3{\cdot}H_2O$ **(2)**
chemical formula weight ($g{\cdot}mol^{-1}$)	392.85	356.82
calculated density ($g{\cdot}cm^{-3}$)	2.015	1.993
crystal system	monoclinic	orthorhombic
space group	$P2_1/m$	$Cmcm$
a (Å)	9.5724(9)	10.3093(4)
b (Å)	7.1632(6)	15.9456(6)
c (Å)	9.9780(9)	7.2219(3)
β (deg)	108.816(5)	
V (Å^3)	647.6(2)	1187.2(1)
figures of merit	$M_{20} = 37$ $F_{20} = 61$	$M_{20} = 103$ $F_{20} = 201$
Z	2	4
radiation (Å)	1.5406−1.5444	1.5406−1.5444
2θ range (deg)	7−77	7−77
no. of reflections	380	201
no. of atoms	17	11
no. of structural parameters	37	22
R_P	0.116	0.103
R_{WP}	0.151	0.132
R_B	0.085	0.088
R_F	0.063	0.082

of these two cells with systematic absences consistent with the $P2_1$ or $P2_1/m$ space groups[29] for **1** and $Cmc2_1$ or $Cmcm$ space groups for **2**. Structure determinations were performed using the EXPO[30] package, which combines a full pattern decomposition program EXTRA[31] and the direct methods program SIR97[32] optimized for powder diffraction data. The centric $P2_1/m$ and $Cmcm$ space groups were chosen to solve the structures of **1** and **2**, respectively.

For **1** and **2**, respectively, 443 and 219 reflections were extracted over the angular range of 7−80° (2θ). According to the degree of diffraction line overlap, 23.5% and 53.0% of these reflections were statistically considered as independent for **1** and **2**, respectively. A pseudo-translational symmetry has been detected in both cases and used as prior information in EXTRA.[31] The first E-map revealed the location of almost all the atoms of the inorganic skeleton (the gallium site, one or two phosphorus sites, and several possible sites for oxygen or fluorine atoms). The overall 1D character of these two structures was clearly defined. The distance between adjacent gallium atoms within a chain was found to be $d_{Ga-Ga} = b/2 = 3.58$ Å for **1** and $d_{Ga-Ga} = c/2 = 3.61$ Å for **2**, which is very similar to those encountered in "tancoite-like" phases: $d_{Ga-Ga} = a/2 = 3.54$ Å for $Ga(HPO_4)_2F{\cdot}N_2C_3H_{12}{\cdot}2H_2O$,[33] $d_{Ga-Ga} = c/2 = 3.54$ Å for $Ga(HPO_4)_2F{\cdot}N_2C_6H_{14}$,[34] $d_{Ga-Ga} = c/2 = 3.56$ Å for $Ga(HPO_4)_2F{\cdot}N_2C_3H_{12}$,[35] $d_{Ga-Ga} = b/2 = 3.56$ Å for $[(1R,2R)\text{-}C_6H_{10}(NH_3)_2][Ga(OH)(HPO_4)_2]{\cdot}H_2O$,[36] $d_{Ga-Ga} = c/2 = 3.58$ Å for $[trans\text{-}1,2\text{-}C_6H_{10}(NH_3)_2][Ga(OH)(HPO_4)_2]{\cdot}H_2O$,[36] and $d_{Ga-Ga} = b/2 = 3.58$ Å for $Na_3Ga(HPO_4)(PO_4)$.[37] By analogy to those phases, it was assumed that, as a starting point for construction of a structural model, the compounds **1** and **2** should contain a zigzag chain of fluorine-sharing $\{GaO_4F_2\}$ octahedra. The corresponding atomic coordinates were used as a starting model in the Rietveld refinement. The pseudo-Voigt function and the usual quadratic function in $\tan\theta$ were used to describe the individual line profile and the angular dependence of the peak full-width at half-maximum, respectively. The Rietveld refinement of these built partial models converged to $R_B = 0.427$ and $R_F = 0.175$ for **1** and $R_B = 0.203$ and $R_F = 0.146$ for **2**. The use of soft distance and angular constraints to regularize the starting structural model gave a slightly clearer difference electron-density map. Further alternate cycles of refinement and successive difference Fourier maps using SHELXL[38] allowed complete location of the template cations and of the occluded water molecules (three water molecules for compound **1** and one water molecule for compound **2** according to the TGA measurement). In the case of compound **2**, two sites were clearly identified for only one water molecule. Then, the occupancy was allowed to vary in the opposite manner with a sum fixed equal to 0.25 (Wyckoff position 4c, see Table 3). Also, a very small amount of compound **1** was detected on the powder diffraction pattern of compound **2** and its most intense diffraction lines were considered as contributing to the overall background. The final Rietveld refinement was carried out over the angular range of 7−77° (2θ) for **1** and **2** by using 380 and 201 reflections, respectively. Details of the two refinements are summarized in Table 2, final non-hydrogen atomic parameters are given in Table 3, and selected bond distances and angles are listed in Table 4. The final Rietveld plots are given in Figure 1.

Structure Description The X-ray structure determinations reveal that the structures of compound **1** and **2** both contain infinite anionic chains of $[Ga(P_2O_7)F]^{2-}$ separated by charge-balancing 1,3-propyldiammonium

(28) Rodriguez-Carvajal, J. In *Collected Abstracts of Powder Diffraction Meeting*, Toulouse, France, 1990; p 127.
(29) *International Tables for Crystallography, Volume A*; Hahn, T., Ed.; Kluwer Academic Publishers: Dordrecht, The Netherlands, 1995.
(30) Altomare, A.; Burla, M. C.; Camalli, M.; Carrozzini, B.; Cascarano, G. L.; Giacovazzo, C.; Guagliardi, A.; Moliterni, A. G. G.; Polidori, G.; Rizzi, R. *J. Appl. Crystallogr.* **1999**, *32*, 339.
(31) Altomare, A.; Burla, M. C.; Cascarano, G. L.; Giacovazzo, C.; Guagliardi, A.; Moliterni, A. G. G.; Polidori, G. *J. Appl. Crystallogr.* **1995**, *28*, 842.
(32) Altomare, A.; Burla, M. C.; Camalli, M.; Cascarano, G. L.; Giacovazzo, C.; Guagliardi, A.; Moliterni, A. G. G.; Polidori, G.; Spagna, R. *J. Appl. Crystallogr.* **1999**, *32*, 115.
(33) Walton, R. I.; Millange, F.; Le Bail, A.; Loiseau, T.; Serre, C.; O'Hare, D.; Férey, G. *Chem. Commun.* **2000**, 203.
(34) Bonhomme, F.; Thoma, S. G.; Nenoff, T. M. *J. Mater. Chem.* **2001**, *11*, 2559.
(35) Walton, R. I.; Millange, F.; O'Hare, D.; Paulet, C.; Loiseau, T.; Férey, G. *Chem. Mater.* **2000**, *12*, 1977.
(36) Lin, H.-M.; Lii, K.-H. *Inorg. Chem.* **1998**, *37*, 4220.
(37) Lii, K.-H.; Wang, S.-L. *J. Solid State Chem.* **1997**, *128*, 21.
(38) *SHELXL97*; University of Göttingen: Göttingen, Germany, 1997.

Table 3. Atomic Coordinates and Isotropic Displacement Parameters (Å²) for Non-hydrogen Atoms

(a) $Ga(P_2O_7)F{\cdot}H_3N(CH_2)_3NH_3{\cdot}3H_2O$ (**1**)

atom	*x*	*y*	*z*	B_{iso}
Ga	0	0	0	0.28(2)
P1	0.2092(9)	1/4	0.2534(8)	0.38(3)[a]
P2	0.2671(8)	1/4	−0.0095(8)	0.38(3)[a]
F	−0.078(2)	1/4	−0.031(2)	2.4(3)[b]
O1	0.320(1)	1/4	0.1578(9)	2.4(3)[b]
O2a	0.295(2)	1/4	0.408(1)	2.4(3)[b]
O2b	0.392(2)	1/4	−0.069(3)	2.4(3)[b]
O3a	0.120(1)	0.075(1)	0.215(2)	2.4(3)[b]
O3b	−0.168(2)	−0.084(2)	0.055(2)	2.4(3)[b]
N1	−0.126(3)	1/4	0.655(2)	2.8(5)[c]
C1	−0.101(1)	1/4	0.5181(9)	2.8(5)[c]
C2	−0.244(1)	1/4	0.4070(9)	2.8(5)[c]
C3	−0.212(1)	1/4	0.2730(9)	2.8(5)[c]
N2	−0.351(2)	1/4	0.156(2)	2.8(5)[c]
Ow1	0.621(3)	1/4	0.837(3)	4[d]
Ow2	0.182(3)	1/4	0.621(3)	4[d]
Ow3	1/2	0	1/2	4[d]

(b) $Ga(P_2O_7)F{\cdot}H_3N(CH_2)_3NH_3{\cdot}H_2O$ (**2**)

atom	*x*	*y*	*z*	B_{iso}	occupancy
Ga	0	0	0	1.75(9)	1/4
P	0.1428(5)	0.1345(4)	1/4	2.3(2)	1/2
F	0	−0.0505(8)	1/4	2.1(2)[e]	1/4
O1	0	0.1834(9)	1/4	2.1(2)[e]	1/4
O2	0.2472(9)	0.2000(6)	1/4	2.1(2)[e]	1/2
O3	0.1336(6)	0.0812(3)	0.4318(9)	2.1(2)[e]	1
C1	0.1151(7)	0.4204(6)	1/4	2.7(3)[f]	1/2
C2	0	0.3702(9)	1/4	2.7(3)[f]	1/4
N	0.231(1)	0.3646(7)	1/4	2.7(3)[f]	1/2
Ow1	1/2	0.283(4)	1/4	4[g]	0.061(2)[h]
Ow2	1/2	0.131(1)	1/4	4[g]	0.189(2)[h]

[a−c] Allowed to vary in the same manner. [d] Fixed. [e−f] Allowed to vary in the same manner. [g] Fixed. [h] Allowed to vary in the opposite manner.

cations and occluded water molecules (see Figure 2). The backbone of the chains consists of $\{GaO_4F_2\}$ octahedra sharing trans (F) vertexes running along [010] and [001] for **1** and **2**, respectively (see Figures 2 and 3). In both cases, octahedra are almost regular with Ga−O (and/or Ga−F) distances ranging from 1.927(8) to 2.15(2) Å for **1** and from 1.953(6) to 1.977(5) Å for **2**. The remaining four oxygen atoms are shared with $\{P_2O_7\}$ diphosphate groups; the octahedra making up the spine of the chain are tilted in such a way that each diphosphate group links two adjacent octahedra (see Figure 4). Then, these phosphorus polyhedra bridge pairs of gallium octahedra along the chain on both sides. In both structures, phosphorus atoms are tetrahedrally coordinated with P−O distances ranging from 1.50(1) to 1.64(1) Å for **1** and from 1.50(1) to 1.666(9) Å for **2**. Two phosphate groups are linked together to form a P_2O_7 unit, via the oxygen corner which corresponds obviously to the longest P−O distance observed (see Table 4 and Figure 4, P1−O1 and P2−O1 for **1** and P−O1 for **2**). The P−O−P angles observed (124(1)° and 124.2(6)° for **1** and **2**, respectively) are typical for diphosphate-containing materials: for example, in a one-dimensional fluorinated nickel diphosphate the P−O−P angle is 126.2(2)°,[39] and in a vanadium phosphate−diphosphate material the P−O−P angle is 121.5(2)°.[40] The diaminopropane molecules lie between the resulting chains of

(39) Liu, Y.; Zhang, L.; Shi, Z.; Yuan, H.; Pang, W. *J. Solid State Chem.* **2001**, *158*, 68.

(40) Chippindale, A. M. *Chem. Mater.* **2000**, *12*, 818.

Table 4. Selected Bonds Lengths (Å) and Angles (deg)

(a) $Ga(P_2O_7)F{\cdot}H_3N(CH_2)_3NH_3{\cdot}3H_2O$ (**1**)

Within the GaO_4F_2 Octahedron

Ga−F (×2)	1.927(8)
Ga−O3b (×2)	1.95(2)
Ga−O3a (×2)	2.15(2)
F−Ga−F	180
F−Ga−O3a (×2)	89(1)
F−Ga−O3a (×2)	91(1)
F−Ga−O3b (×2)	91(1)
F−Ga−O3b (×2)	89(1)
O3a−Ga−O3a	180
O3a−Ga−O3b (×2)	91(1)
O3a−Ga−O3b (×2)	89(1)
O3b−Ga−O3b	180

Within the Diphosphate Groups

P1−O3a (×2)	1.50(1)	P2−O3b(×2)	1.50(1)
P1−O1	1.64(1)	P2−O1	1.58(1)
P1−O2a	1.50(1)	P2−O2b	1.50(2)
O3a−P1−O3a	114(1)	O3b−P2−O3b	105(1)
O3a−P1−O1 (×2)	106(1)	O3b−P2−O1 (×2)	106(1)
O3a−P1−O2a (×2)	110(1)	O3b−P2−O2b (×2)	113(1)
O1−P1−O2a	111(1)	O1−P2− O2b	113(1)
		P1−O1−P2 124(1)	

Within the Organic Part

N1−C1	1.46(2)	N1−C1−C2	109(1)
C1−C2	1.45(1)	C1−C2−C3	106(1)
C2−C3	1.46(1)	C2−C3−N2	109(2)
C3−N2	1.46(1)		

Most Probable Hydrogen Bonds

N1.....O3a (×2)	2.66(1)
N1.....F	3.02(1)
N1.....Ow2	3.08(3)
N2.....O2b	2.75(1)
N2.....Ow1	3.11(3)
N2.....O1	3.16(3)
Ow1.....F	2.75(3)
Ow1.....O2b	2.65(3)
Ow2.....O2a	2.68(3)
Ow2.....O2b	3.10(3)
Ow3.....O2a (×2)	2.59(1)

(b) $Ga(P_2O_7)F{\cdot}H_3N(CH_2)_3NH_3{\cdot}H_2O$ (**2**)

Within the GaO_4F_2 Octahedron

Ga−O3 (×4)	1.953(6)
Ga−F (×2)	1.977(5)
F−Ga−F	180
F−Ga−O3 (×4)	92.3(5)
F−Ga−O3 (×4)	87.7(4)
O3−Ga−O3 (×2)	90.3(4)
O3−Ga−O3 (×2)	89.7(4)
O3−Ga−O3 (×2)	180

Within the Diphosphate Group

P−O1	1.666(9)
P−O2	1.50(1)
P−O3 (×2)	1.567(7)
O1−P−O2	108.0(8)
O1−P−O3 (×2)	101.6(7)
O2−P−O3 (×2)	114.9(8)
O3−P−O3	113.9(7)
P−O1−P	124.2(6)

Within the Organic Part

C1−C2	1.43(1)
C1−N	1.49(1)
C1−C2−C1	112.0(9)
C2−C1−N	109.3(9)

Most Probable Hydrogen Bonds

N.....F	3.09(1)
N.....O2	2.63(1)
N.....O3 (×2)	2.825(9)
N.....Ow1 (×2)	3.06(3)
Ow1....F	2.66(7)
Ow1....O2 (×2)	2.92(3)
Ow1....N (×2)	3.06(3)
Ow2....O2 (×2)	2.83(1)

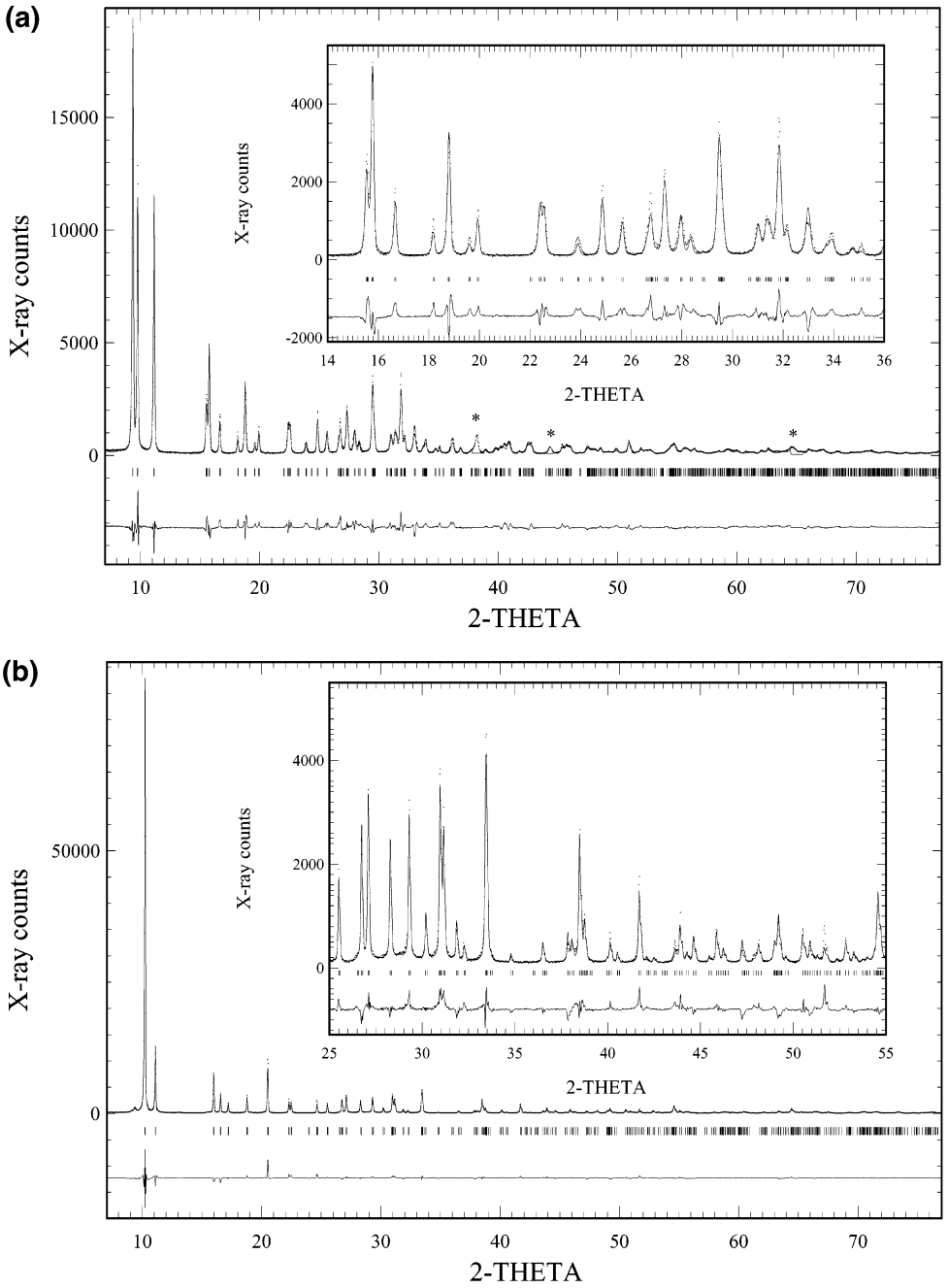

Figure 1. Final Rietveld refinement plot for (a) $Ga(P_2O_7)F{\cdot}H_3N(CH_2)_3NH_3{\cdot}3H_2O$ (**1**) and for (b) $Ga(P_2O_7)F{\cdot}H_3N(CH_2)_3NH_3{\cdot}H_2O$, (**2**). Observed, calculated, and difference profiles are plotted on the same scale. Bragg peaks are indicated by tick marks. Inset is an expanded region of a small part of the data. A star indicates the sample holder.

$[GaP_2O_7F]^{2-}$ and are protonated twice to balance the two negative charges of the inorganic chain. An extensive network of hydrogen bonds thus contributes to the cohesion of these two compounds through template−chain, occluded water−chain, and finally occluded water−template interactions (see Table 4).

The topology of the chains in $Ga(P_2O_7)F{\cdot}H_3N(CH_2)_3NH_3{\cdot}3H_2O$, **1**, and $Ga(P_2O_7)F{\cdot}H_3N(CH_2)_3NH_3{\cdot}H_2O$, **2**, is identical, but the arrangement of the template molecule between the chains is slightly different since, in the highest hydrated form, three water molecules are found between the chains. The phase transition between **1** and **2** induced by the total loss of the water molecule Ow3 and the partial loss of Ow1 and Ow2 can be considered as a topotactic transformation a priori. The unchanged inorganic chains and amines, seen in both compounds, are due to the conservation of the centers of symmetry of the monoclinic cell in the orthorhombic one. During the dehydration, a clockwise rotation of approximately 25° for the amines and of about 9° for the inorganic chains are observed in the (010) plane in the monoclinic system. Therefore, the chains are closer to each other in compound **2**.

When applied to a structure determined by powder diffraction data, bond valence sum (BVS) calculations[41] are of limited accuracy due to the inherent imprecision of bond distances. Nevertheless, BVS calculations confirm that in both compounds the gallium and the phosphorus atoms have essentially the expected va-

(41) Brese, N. E.; O'Keeffe, M. *Acta Crystallogr., Sect. B* **1991**, *47*, 192.

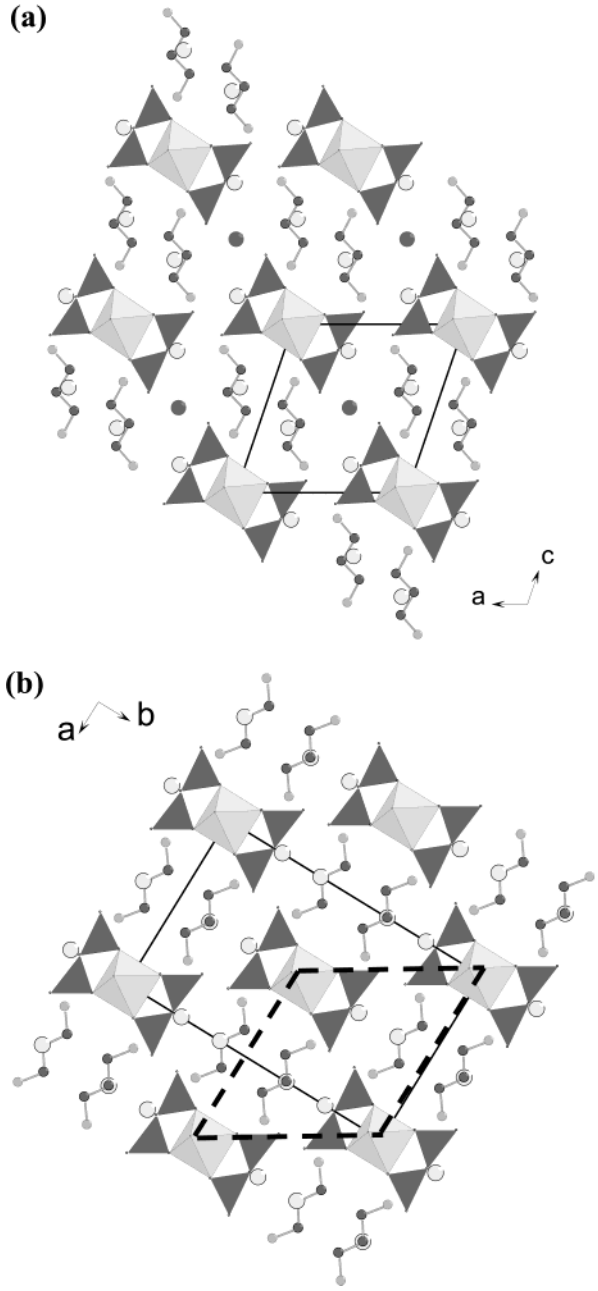

Figure 2. (a) A polyhedral view of the structure of $Ga(P_2O_7)F\cdot H_3N(CH_2)_3NH_3\cdot 3H_2O$ (**1**) along the *b* axis. **(b)** A polyhedral view of the structure of $Ga(P_2O_7)F\cdot H_3N(CH_2)_3NH_3\cdot H_2O$ (**2**) along the *c* axis. Dark gray polyhedra are phosphorus tetrahedra and light gray polyhedra $\{GaO_4F_2\}$ octahedra. Large circles (light and dark gray for (**1**) and light gray for (**2**)) are occluded water molecules and small circles are carbon (dark gray) and nitrogen (medium gray). A continuous dark line shows the unit cells. The faint line shows the corresponding monoclinic cell for (**2**).

lences. To our knowledge, the topology of the $[GaP_2O_7F]^{2-}$ chains has not previously been observed for an anionic gallium phosphate with organic counterions. The linking of $\{MO_4F_2\}$ octahedral units to form a zigzag chain has been reported for several compounds, the archetypal example being the mineral tancoite, $LiNa_2HAl(PO_4)_2(OH)$,[42] but also in synthetic aluminum and gallium phosphates[36,37,43] and in transition-metal phosphates.[44−46]

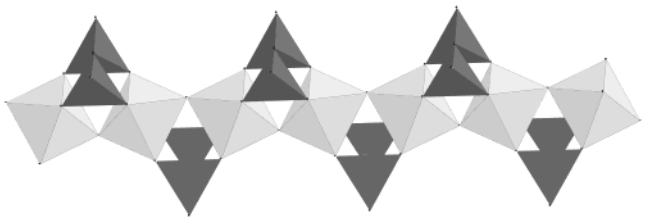

Figure 3. Part of the infinite chain found in $Ga(P_2O_7)F\cdot H_3N(CH_2)_3NH_3\cdot 3H_2O$ (**1**) and $Ga(P_2O_7)F\cdot H_3N(CH_2)_3NH_3\cdot H_2O$ (**2**).

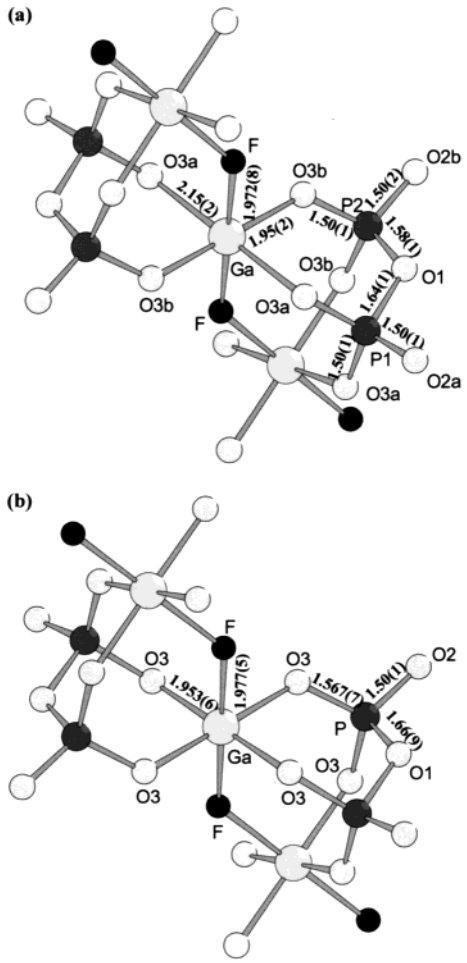

Figure 4. Schematic "balls and sticks" representation of the connection mode of polyhedra within the inorganic chains of (a) $Ga(P_2O_7)F\cdot H_3N(CH_2)_3NH_3\cdot 3H_2O$ (**1**) and (b) $Ga(P_2O_7)F\cdot H_3N(CH_2)_3NH_3\cdot H_2O$ (**2**).

The tancoite-type materials, however, all contain isolated $\{PO_4\}$ units.

Thermal Properties. The thermal stability of **1** and **2** was examined by thermogravimetry analysis (TGA) and variable-temperature powder X-ray diffraction (HTXRD). The TG curves exhibit two significant mass changes over the temperature ranges 25−80 °C and 300/350−600 °C (Figure 5). Thermogravimetric analyses are

(42) Hawthorne, F. C. *Tschermaks Mineral. Petrogr. Mitt.* **1983**, *31*, 121.

(43) Attfield, M. P.; Morris, R. E.; Burshtein, I.; Campana, C. F.; Cheetham, A. K. *J. Solid State Chem.* **1995**, *118*, 412.

(44) Zhang, Y.; Warren, C. J.; Clearfield, A.; Haushalter, R. C. *Polyhedron* **1998**, *17*, 2575.

(45) Lethbridge, Z. A. D.; Lighfoot, P.; Morris, R. E.; Wragg, D. S.; Wright, P. A.; Kvick, A.; Vaughan, G. *J. Solid State Chem.* **1999**, *142*, 455.

(46) Cavellec, M.; Riou, D.; Grenèche, J. M.; Férey, G. *Inorg. Chem.* **1997**, *36*, 2187.

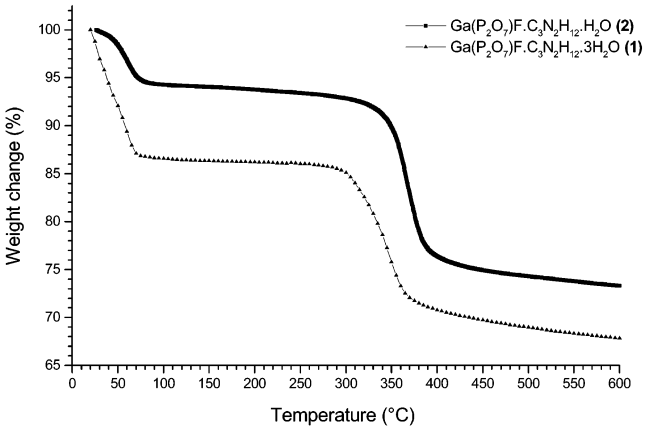

Figure 5. Thermogravimetric analyses for $Ga(P_2O_7)F{\cdot}H_3N(CH_2)_3NH_3{\cdot}3H_2O$ (**1**) and $Ga(P_2O_7)F{\cdot}H_3N(CH_2)_3NH_3{\cdot}H_2O$ (**2**).

in agreement with the formulation of $Ga(P_2O_7)F{\cdot}H_3N(CH_2)_3NH_3{\cdot}3H_2O$, **1**, and $Ga(P_2O_7)F{\cdot}H_3N(CH_2)_3NH_3{\cdot}H_2O$, **2**, respectively. For **1**, a first weight loss of 13.5% occurs below 100 °C and corresponds to the loss of occluded water in the structure (expected 13.7%). The removal of the 1,3-diaminopropane molecule is observed between 300 and 600 °C (observed 19.0%; calculated 22.4%). The TG curve of **2** shows similar behavior. The first weight loss at low temperature (T < 100 °C) is attributed to the loss of water (observed 5.6%; calculated 5.1%). Between 350 and 600 °C a gradual mass loss of 21.0% is consistent with the loss of amine (expected 22.4%). Once the less hydrated material **2** has lost water, its thermal behavior is remarkably similar to that of **1**. Moreover, the slight inflection point observed on the TGA of compound **1** around 50 °C could be ascribed to the transformation into **2** as pointed out by the HTXRD (see section below).

The determination of crystalline phases formed during calcination at various temperatures is useful for assessing the thermal stability of the materials. A general view (Figure 6) shows the whole HTXRD plot of $Ga(P_2O_7)F{\cdot}H_3N(CH_2)_3NH_3{\cdot}3H_2O$, **1**. First, variable-temperature powder X-ray diffraction studies of **1** show that crystallinity is retained upon the loss of water. There are four temperature regions, which are classified by a common HTXRD plot in each region: 30−50, 50−80, 80−420, and 420−600 °C. Sharp and intense patterns were observed in the first three temperature regions. On calcination up to 50 °C (the first region), the continuous removal of two water molecules per formula leads to $Ga(P_2O_7)F{\cdot}H_3N(CH_2)_3NH_3{\cdot}H_2O$, **2**. Between 50 and 80 °C, the structure of $Ga(P_2O_7)F{\cdot}H_3N(CH_2)_3NH_3{\cdot}H_2O$, **2**, remains. When the sample is calcined between 80 and 420 °C, the XRD patterns have slightly weaker and broader diffraction features, but a new set of Bragg peaks are distinctly observed. We assume these are due to anhydrous $Ga(P_2O_7)F{\cdot}H_3N(CH_2)_3NH_3$. We have synthesized a material of this composition and measured diffraction data which correspond to the peaks seen in the thermodiffractometry experiment (a = 10.743(3) Å, b = 7.957(3) Å, c = 7.183(3) Å, α = 94.50(4)°, β = 121.67(4)°, γ = 96.08(4)°) but as yet a structure solution has not been successfully performed. On increasing the temperature further, the absence of diffraction peaks corresponding to this phase shows that the structure is destroyed completely with the removal of the 1,3-diaminopropane molecule. No major changes are observed as the calcination temperature is increased up to 600 °C. It should be mentioned that at higher temperatures (for example, 1000 °C) the XRD patterns correspond to dense gallium phosphate with the low cristobalite structure type, $GaPO_4$.

Hydrothermal Behavior of the Materials. During in situ EDXRD studies of the hydrothermal crystallization of the 3D open-framework phase ULM-3, $Ga_3(PO_4)_3F_2{\cdot}H_3N(CH_2)_3NH_3{\cdot}H_2O$, from an aqueous mixture

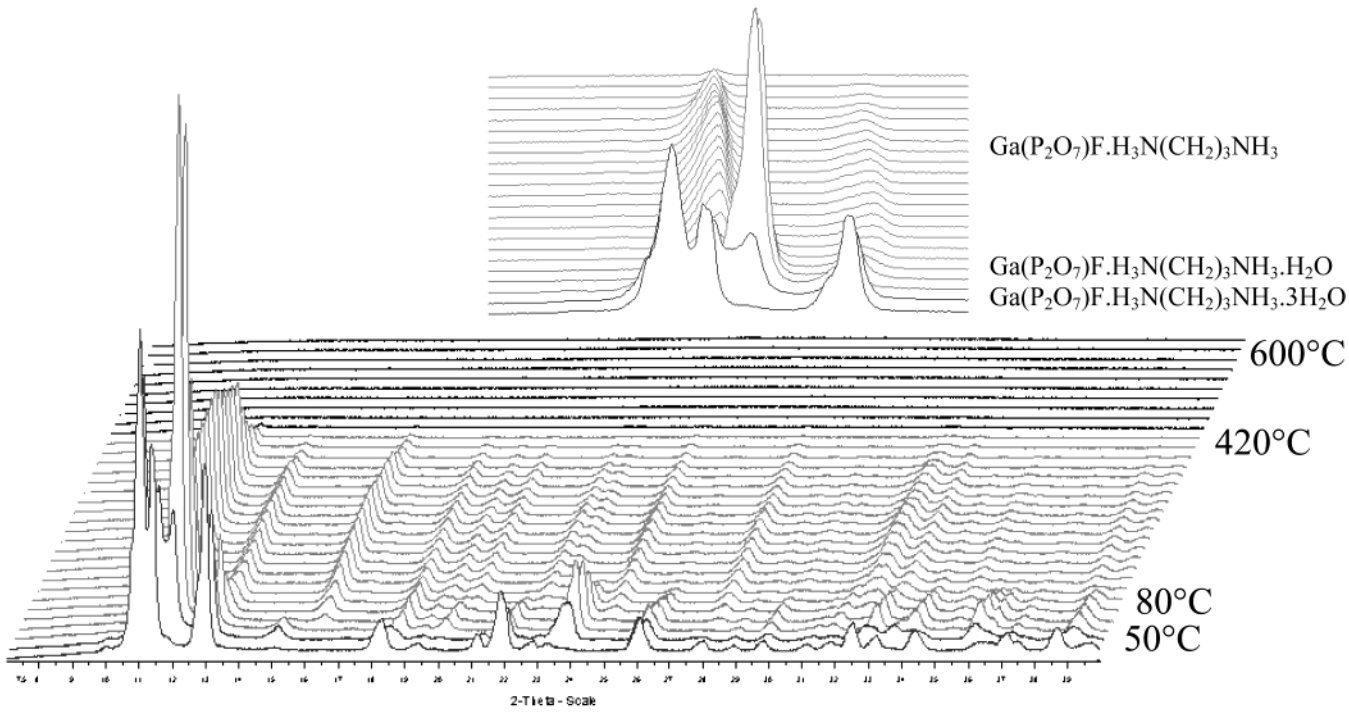

Figure 6. In situ HTXRD diffraction patterns of $Ga(P_2O_7)F{\cdot}H_3N(CH_2)_3NH_3{\cdot}3H_2O$ (**1**) between 30 and 600 °C (temperature steps of 10 °C from 30 to 100 °C and of 20 °C thereafter up to 600 °C). Inset is an expanded region of a small part of the data.

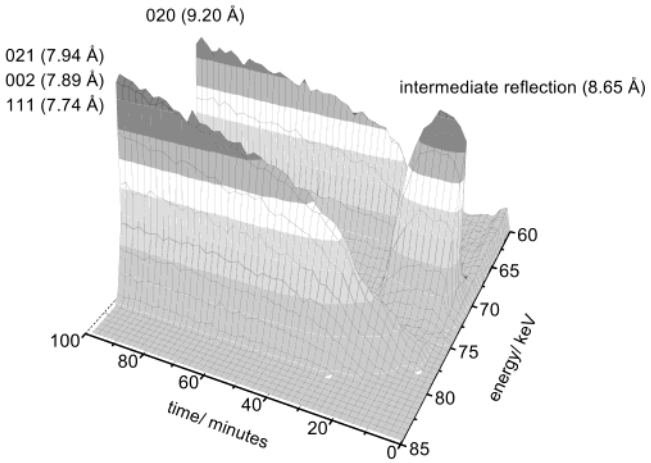

Figure 7. A small part of energy-dispersive X-ray diffraction data (30-s intervals) measured in situ during the crystallization of the open-framework gallium fluorophosphate ULM-3 from an amorphous phosphate gel at 180 °C. The use of P_2O_5 as a reagent results in the formation of a crystalline intermediate phase identified as $Ga(P_2O_7)F{\cdot}H_3N(CH_2)_3NH_3{\cdot}H_2O$ (**2**) before the onset crystallization of the product.

Table 5. Observed Bragg Reflections of the Transient Intermediate Seen in the in Situ EDXRD Study, d_{obs}, with the Corresponding First 26 Reflections of the Powder Pattern of $Ga(P_2O_7)F{\cdot}H_3N(CH_2)_3NH_3{\cdot}H_2O$ (2)

d_{obs}	d_{calc}	(hkl)	d_{obs}	d_{calc}	(hkl)	d_{obs}	d_{calc}	(hkl)
8.66	8.659	(110)		3.713	(221)	2.95	2.958	(202)
8.00	7.975	(020)	3.59	3.611	(002)	2.88	2.890	(241)
5.54	5.547	(111)	3.49	3.490	(041)		2.890	(330)
5.35	5.354	(021)		3.359	(310)	2.86	2.869	(132)
5.15	5.155	(200)	3.32	3.33	(112)	2.81	2.807	(151)
4.74	4.725	(130)	3.28	3.289	(022)	2.77	2.772	(222)
4.34	4.329	(220)	3.16	3.153	(240)	2.67	2.680	(331)
3.99	3.986	(040)	3.04	3.046	(150)		2.680	(042)
3.95	3.954	(131)		3.046	(311)			

of Ga_2O_3, P_2O_5, $H_2N(CH_3)_2NH_2$, and HF, we have previously reported the observation of a transient crystalline phase.[15] With the use of a novel three-element detector we are now able to assign, unambiguously, all of the transient diffraction features to compound **2**. Figure 7 shows the in situ diffraction data measured by one detector during the hydrothermal crystallization of ULM-3 at 180 °C. These data clearly show the presence of the crystalline intermediate phase. Using the data from two detectors, we can now identify this phase as compound **2**; Table 5 shows the *d* spacings of diffraction peaks observed in situ, obtained by using the peak-fitting software XFIT[47] with a pseudo-Voigt function, along with the calculated peak positions. This is an excellent example of how the large extent of in situ data now available from the multi-detector-element EDXRD technique permits phase identification. At 180 °C **2** is present during the hydrothermal formation of ULM-3 for around 40 min, but if the temperature is lowered to 140 °C, the intermediate is observed for over 2 h.[15] In earlier attempts to isolate **2** by quenching to room temperature the reaction at 140 °C at the point at which the peaks of the crystalline phase had reached their maximum intensity, we observed transformation to a second crystalline phase, even before the hydrothermal autoclave had been opened and the solid

(47) Cheary, R. W.; Coelho, A. A. *J. Appl. Crystallogr.* **1992**, *25*, 109.

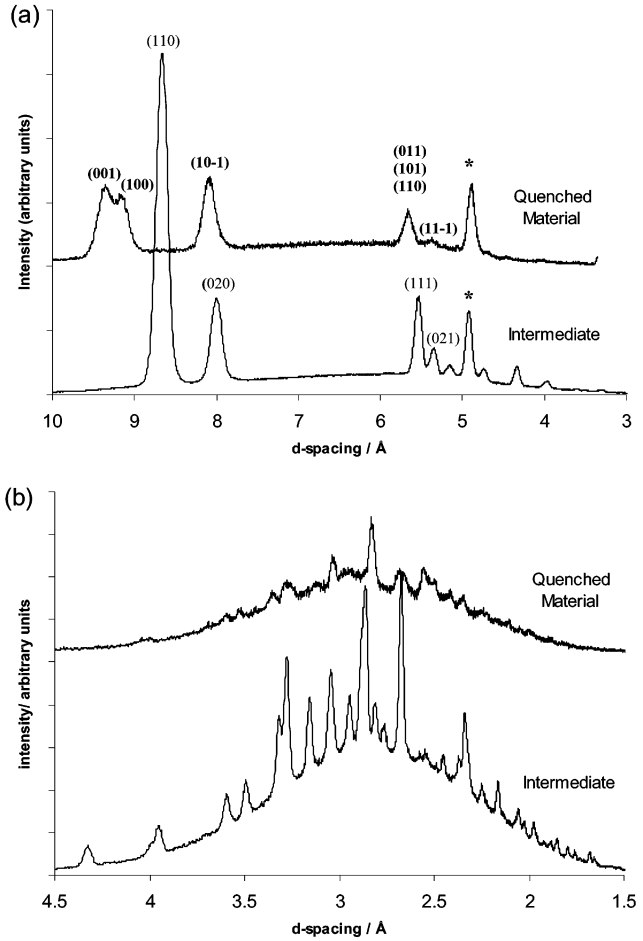

Figure 8. EDXRD diffraction patterns measured from the transient intermediate phase (in situ at 140 °C) and the phase produced after quenching the reaction mixture to room temperature. A star indicates the Teflon bomb.

Table 6. Observed Bragg Reflections, d_{obs}, of the Crystalline Phase Produced on the Quenching Transient Intermediate Seen in the in Situ EDXRD Study with the Corresponding First 39 Reflections of the Powder Pattern of $Ga(P_2O_7)F{\cdot}H_3N(CH_2)_3NH_3{\cdot}3H_2O$ (1)

d_{obs}	d_{calc}	(hkl)	d_{obs}	d_{calc}	(hkl)
9.40	9.447	(001)	3.35	3.349	(021)
9.12	9.061	(100)		3.331	(120)
8.07	7.942	(10−1)		3.325	(10−3)
5.66	5.707	(011)		3.304	(112)
	5.686	(101)	3.28	3.265	(12−1)
	5.619	(110)		3.253	(211)
5.37	5.319	(11−1)		3.191	(30−1)
4.84	4.883	(10−2)	3.12	3.148	(003)
4.68	4.722	(002) and (20−1)		3.095	(20−3)
4.48	4.530	(200)	3.03	3.031	(121)
	4.454	(111)		3.026	(30−2)
3.99	4.035	(11−2)		3.020	(300)
	3.971	(20−2)	2.97	3.016	(11−3)
	3.943	(012)		2.915	(31−1)
	3.942	(21−1)		2.888	(12−2)
	3.829	(210)		2.882	(013)
3.71	3.724	(102)	2.84	2.854	(022)
3.59	3.651	(201)	2.83	2.854	(22−1)
	3.582	(020)		2.843	(202)
3.53	3.473	(21−2)		2.841	(21−3)

recovered. Figure 8 shows the total accumulated EDXRD data from both **2** and the transformed material produced on cooling. We can now identify the transformed material as compound **1**, and Table 6 shows the indexed

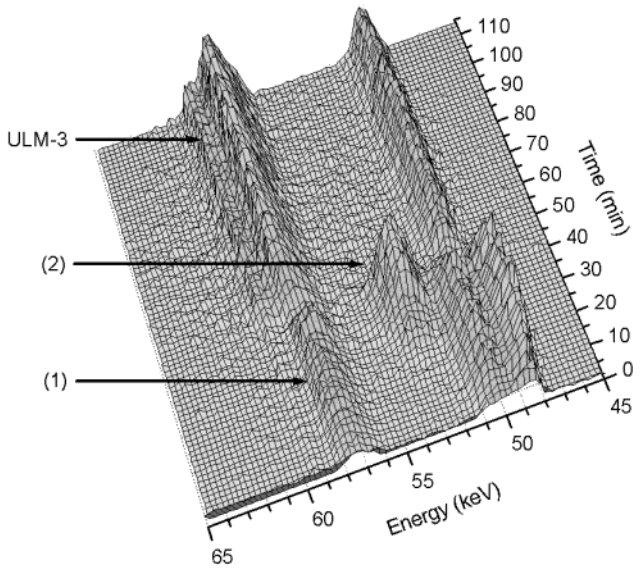

Figure 9. EDXRD data recorded in situ as $Ga(P_2O_7)F{\cdot}H_3N(CH_2)_3NH_3{\cdot}3H_2O$ (**1**) is heated with water in the hydrothermal bomb. The formation of a crystalline intermediate phase identified as $Ga(P_2O_7)F{\cdot}H_3N(CH_2)_3NH_3{\cdot}H_2O$ (**2**) is shown by a stack plot of the data before the onset crystallization of the final product ULM-3.

powder diffraction data measured from within the hydrothermal cell.

If the hydrothermal autoclave is returned to the in situ diffraction apparatus after transformation to **1** has taken place and the mixture reheated, then reconversion to **2** is observed, followed by further conversion into ULM-3 (Figure 9). Conclusive confirmation of the correct identification of phases **1** and **2** is given by the fact that solid **1**, prepared by room-temperature crystallization, is heated in water; stepwise transformation to ULM-3 via **2** is observed. It should be noted that this process requires the addition of no extra reagents; compound **1** is clearly metastable with respect to **2**, its more dehydrated form, which in turn is metastable with respect to microporous ULM-3. To gain more information about this transformation process, we have determined the changing areas of the strongest Bragg peaks of **1**, **2**, and ULM-3 during the hydrothermal conversion using a heating rate of ~3 °C min^{-1} from 20 °C. The most intense peaks of **1**, (100) and (001), and **2**, (010), are well-resolved, but the most intense peaks of ULM-3 overlap considerably with those of both **1** and **2**, so we have studied here a weaker diffraction feature (the closely separated 212 and 102 peaks). The resulting temporal profiles are shown in Figure 10. These peak intensity data correspond to crystallization curves since the area of a Bragg peak is directly proportional to the amount of diffracting solid. Although kinetic analysis of such data is extremely difficult and would require information from other techniques concerning the chemical processes occurring in solution before and during the transformations, we can draw some important conclusions. Compound **1** is stable in solution until a temperature of 120 °C is reached, and then its decay takes place over a 15-min period, being complete once a temperature of 195 °C is attained. Interestingly, compound **2** appears almost as soon as **1** begins to decay, but also its Bragg peaks continue to increase in intensity for a considerable time after **1** has been totally consumed. Another feature of the data that is important to note is the temporary halt in growth of **2** from 50 to 62 min; this corresponds to the time in which **1** is in the final stages of decay and suggests that the final dissolution of **1** releases reactive solution species to allow the continued growth of **2**. The continued growth of **2** (~20 min) after the disappearance of **1** is consistent with this postulated dissolution model.

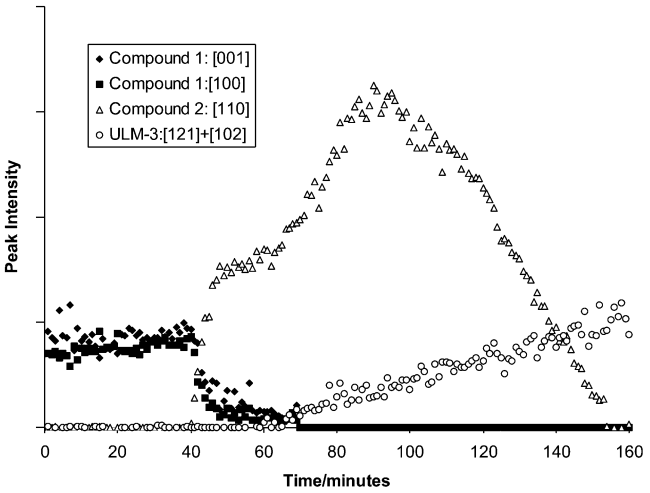

Figure 10. Crystallization curves determined by peak area determination of Bragg reflections of **1**, **2**, and ULM-3 during the hydrothermal transformation of **1** to ULM-3 via **2**.

Discussion

The isolation of disphosphate-containing solids from reaction mixtures treated using mild hydrothermal conditions is extremely unusual. In the past 20 years hundreds of new phosphates have been synthesized using hydrothermal chemistry, and the vast majority of these contain isolated $\{PO_4\}$ units with oxide vertexes shared with those of metal polyhedra or as terminal P−OH or P═O groups. To our knowledge, there are very few reports of the hydrothermal synthesis of disphosphate-containing solids. Two such materials with one-dimensional structures have been reported: Chippindale recently described the synthesis of chain vanadium and gallium phosphate−diphosphates[40] and Liu et al. prepared $Ni(HP_2O_7)F{\cdot}C_2N_2H_{10}$, a material with a similar chain topology to **1** and **2** but with no occluded water molecules.[39] Other synthetic hydrothermal diphosphate materials include layered $H_3OVP_2O_7$,[48] layered $Na_2CrP_2O_7{\cdot}0.5H_2O$,[49] and $CdBa_2(P_2O_7)(HPO_4)$, which contains trigonal prismatic $\{CdO_6\}$ units.[50] The rarity of hydrothermally prepared disphosphate-containing solids must be ascribed to the strongly acidic conditions typically employed in synthesis, as this would bring about hydrolysis of the P−O−P linkages. Indeed, our work shows that **1** and **2** are both metastable in aqueous phase with respect to a phosphate phase and can only be isolated when mild (T < 100 °C) reaction conditions, or a mixed organic−aqueous solvent system, are used. Additionally, P_2O_5 *must* be used as the phosphorus

(48) Badraoui, A. E.; Pivan, J. Y.; Maunaye, M.; Louër, M.; Louër, D. *J. Alloys Compd.* **1996**, *245*, 47.
(49) Stock, N.; Férey, G.; Cheetham, A. K. *Solid State Sci.* **2000**, *2*, 307.
(50) Taher, L. B.; Smiri, L.; Laligant, Y.; Le Bail, A. *Solid State Sci.* **2000**, *2*, 285.

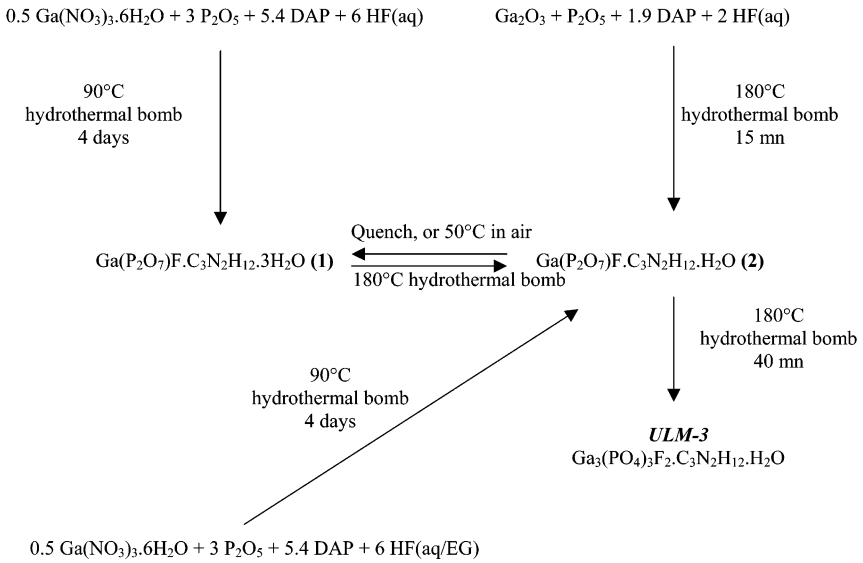

Figure 11. Schematic of the syntheses of and interconversion among $Ga(P_2O_7)F{\cdot}H_3N(CH_2)_3NH_3{\cdot}3H_2O$ (**1**), $Ga(P_2O_7)F{\cdot}H_3N(CH_2)_3$-$NH_3{\cdot}H_2O$ (**2**), and ULM-3 $Ga_3(PO_4)_3F_2{\cdot}H_3N(CH_2)_3NH_3{\cdot}H_2O$.

source for **1** and **2**; presumably some of the P−O−P linkages in this solid are retained in the chain gallium fluorodiphosphates.

Figure 11 summarizes the interconversion routes between **1**, **2**, and ULM-3, with the reaction conditions employed for the synthesis of each phase. The in situ studies reveal that during hydrothermal treatment, the decay of **1** and growth of **2** are closely related. Given that the growth of less hydrated phase **2** continues significantly after **1** is totally consumed, we suggest that the transformation involves a significant amount of dissolution of the starting material. This process is likely to retain the $Ga(P_2O_7)F^{2-}$ chains that are present in both **1** and **2**. We do note, however, that when compound **1** is isolated, the transformation can be affected by heating in dry air, and so that solid−solid conversion is possible. It is probable that the process can take place by either mechanism depending on the reaction conditions used. The conversion of the chain phase **2** into the 3D open-framework material ULM-3 requires considerable atomic rearrangement since whereas **2** contains solely octahedral $\{GaO_4F_2\}$ units, ULM-3 is made up of both$\{GaO_4F_2\}$octahedral units, and $\{GaO_4F\}$ five-coordinate gallium centers. Additionally, the P−O−P linkage of the $\{P_2O_7\}$ unit in **2** must be cleaved to form the isolated $\{PO_4\}$ tetrahedral found in ULM-3. This process is therefore even more likely to be solution-mediated. The transformation of six-coordinate gallium centers into five- and four-coordinate centers in hydrothermal solutions conditions has been observed by in situ NMR studies,[14,51,52] and this backs up our supposition of a solution-mediated transformation of **2** to ULM-3 involving a hydrothermal modification of coordination number.

It is important to note that the one-dimensional diphosphates that we have isolated are not true intermediates in the formation of ULM-3 since they are only observed when P_2O_5 is used as the phosphorus source and not when orthophosphoric acid, H_3PO_4, is used.[15] The phases **1** and **2** are simply competing products during the formation of ULM-3, being formed under hydrothermal conditions, and they dissolve to supply the prenucleation building units in solution prior to the crystallization of the thermodynamically more stable 3D material. It is noteworthy that the transformation of low-dimensional networks (chain and layered) into three-dimensional, open-framework architectures has received considerable recent interest as a model for the crystallization of zeotype phosphates. Ozin and co-workers first put forward the model to explain the formation of aluminum phosphates;[18] this was based on the isolation of a 1D chain that underwent a solid−solid transformation into a layered aluminum phosphate,[53] and by observation of structural similarities in the crystal structures of the aluminum phosphates. The proposed model supposes a "parent" 1D chain constructed from $\{AlO_4\}$ and $\{PO_4\}$ tetrahedra, which undergoes stepwise sequences of hydrolysis of Al−O−P linkages followed by a rotational transformation and condensation to yield new chain, layered, and 3D structures. Other workers have assumed this model for aluminum phosphate formation,[54,55] but there is very little experimental evidence to back it up, and certainly no in situ data have been recorded to substantiate the model as being reasonable. Rao and co-workers studied the formation of zinc phosphates and proposed an *aufbau* model for the building up of three-dimensional structures from monomeric and chain phases.[19] In this case, some of us have provided in situ data that back up this model as a likely route for the crystallization of 3D phases,[56] and ex situ studies of the reactivity of the low-dimensional solids has given corroboratory results.[57,58] The results we present here further demon-

(51) Taulelle, F. *Curr. Opin.. Solid State Mater. Sci.* **2001**, *5*, 397.
(52) Taulelle, F.; Haouas, M.; Gérardin, C.; Estournes, C.; Loiseau, T.; Férey, G. *Colloids Surf. A* **1999**, *158*, 299.
(53) Oliver, S.; Kuperman, A.; Lough, A.; Ozin, G. A. *Chem. Mater.* **1996**, *8*.
(54) Yu, J.; Li, J.; Sugiyama, K.; Togashi, N.; Terasaki, O.; Hiriga, K.; Zhou, B. *Chem. Mater.* **1999**, *11*, 1727.
(55) Vidal, L.; Marichal, C.; Gramlich, V.; Patarin, J.; Gabelica, Z. *Chem. Mater.* **1999**, *11*, 2728.
(56) Walton, R. I.; Norquist, A. J.; Neeraj, S.; Natarajan, S.; Rao, C. N. R.; O'Hare, D. *Chem. Commun.* **2001**, 1990.
(57) Choudhury, A.; Neeraj, S.; Natarajan, S.; Rao, C. N. R. *J. Mater. Chem.* **2002**, *12*, 1004.

strate that metastable 1D phosphates can crystallize during the hydrothermal synthesis of 3D phosphates; in our case, however, the metastable materials act as reservoirs of reagents for further crystallizations to take place, rather than being true reaction intermediates.

Conclusions

The use of mild hydrothermal reaction conditions has allowed the synthesis of new examples of diphosphate-containing materials, including a material previously only seen as a transient, metastable phase during hydrothermal crystallization. With a combination of ab initio structure solution from laboratory powder X-ray diffraction data and time-resolved synchrotron energy-dispersive X-ray diffraction studies, we have been able to determine the structure of the metastable phases and identify them as transient phases during hydrothermal crystallization. This approach will be applicable to the study of hydrothermal syntheses of many microporous molecular sieves and the data potentially used as the basis for models for crystallization mechanism. Future work must utilize in situ monitoring of the species present in solution during the hydrothermal transformations such as those we have studied here; this will then allow a more complete understanding of these complex crystallization processes.

Acknowledgment. We are grateful to the EPSRC for providing access to Daresbury Laboratory and to Dr. S. M. Walker for determining the cell parameters of the single crystal of $[NH_3(CH_2)_3NH_3]P_4O_{12}\cdot 2H_2O$. The authors acknowledge the EPSRC-funded software resource CCP14 for software used in data analysis (http://www.ccp14.ac.uk).

CM021232V

(58) Ayi, A. A.; Choudhury, A.; Natarajan, S.; Neeraj, S.; Rao, C. N. R. *J. Mater. Chem.* **2001**, *11*, 1181.